# Journal of Materials Chemistry A

Accepted Manuscript


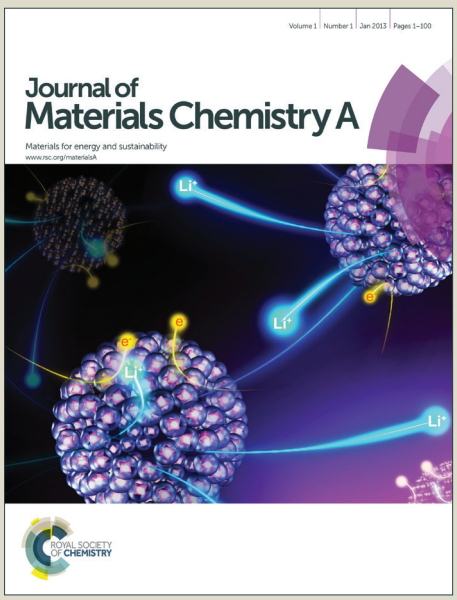





ROYAL SOCIETY OF CHEMISTRY

www.rsc.org/materialsA

Journal Name

COMMUNICATION

# High-performance inverted planar perovskite solar cells without hole transport layer via solution process under ambient condition

Received 00th January 20xx,

Accepted 00th January 20xx

DOI: 10.1039/x0xx00000x

www.rsc.org/

Xichang Bao[a], Qianqian Zhu[a,b], Meng Qiu [a], Ailing Yang[c], Yujin Wang[c], Dangqiang Zhu[a], Junyi Wang [a], and Renqiang Yang[a]*

**High-quality $CH_3NH_3PbI_3$ perovskite films were directly prepared on simple treated ITO glass in air under the relative humidity of lower than 30%. Due to efficient charge transport at the ITO (or PCBM)/$CH_3NH_3PbI_3$ interfaces, the champion and average PCE of 12.78% and 10.85% are obtained in the inverted perovskite solar cells without any hole transport layer, which provides a promising method for low-cost and easy processing industrialization of perovskite solar cells.**

In the past few decades, several promising photovoltaic devices with the advantages of solution-processed, low-cost, and compatible with flexible substrates have attracted considerable attention for next generation renewable energy, such as organic solar cells [1-4], dye sensitized solar cells [5, 6], and quantum dots solar cells [7]. Recently, organometal trihalide perovskites ($CH_3NH_3PbI_3$) are emerging as a new material for photovoltaic applications with above advantages [8-10]. Moreover, this kind of material is abundant in nature and has several promising properties of appropriate band gap, high absorption coefficient, long hole-electron diffusion lengths, excellent carrier transport [11-14]. Great progress has been made in perovskite solar cells, and the power conversion efficiency (PCE) has boosted from 3.8% [15] in 2009 to over 15% [8-10, 16-19]. Now, the highest PCE has reached 20.1% certified by NREL [20]. There are two main architectures considered for perovskite solar cells. One is conventional mesoporous structure commonly using titanium dioxide ($TiO_2$) as electron transport scaffold layer. However, the formation of mesoporous $TiO_2$ layer requires high-temperature processing (>450 $^oC$) to improve charge mobility [21-22], and the resulting device suffers from unstability and exists large hysteresis with different sweep directions[23-24]. Meanwhile, organic material spiro-OMeTAD (2,2',7,7'-tetrakis-(N,N-di-p-methoxyphenylamined)-9,9'-spirobifuorene) is applied as hole transport layer, which needs some additives to improve its performance[23-25]. These further increase the complexity of the device fabrication process. The other device is inverted planar structure, which can avoid using mesoporous $TiO_2$ layer. In the typically inverted structure, poly(3,4-ethylenedioxythiophene:polystyrene sulfonate) (PEDOT:PSS) is the most wildly used as hole transport material on indium tin oxide (ITO) substrate for hole collection and [6,6]-phenyl-C61-butyric acid methyl ester (PCBM) is electron transport layer for electron collection [26-32]. Dai et al reported an inverted $CH_3NH_3PbI_{3-x}Cl_x$ planar perovskite solar cell prepared by layer-by-layer method. The PCE is as high as 15.12% without hysteresis in the current–voltage measurement [29]. However, there are some drawbacks using PEDOT:PSS as hole transport layer due to its hydrophilic and strong acidic nature, which could deteriorate the stability of the solar cells [33-35]. Recently, several groups report inverted perovskite solar cells with nickel oxide ($NiO_x$) as hole transport layer with positive results [36-38]. However, the preparation of $NiO_x$ film requires high-temperature processing or sputtering method, which could increase the cost and complexity of the process. Therefore, it is necessary to develop simple device structures or easy solution-processed hole transport materials for perovskite solar cell applications. One of the challenging and prospective methods is directly fabricating perovskite film on conducting substrate without any transport layer.

In this letter, an inverted planar perovskite solar cell directly prepared on simple treated ITO glass without any hole transport layer was reported. The perovskite films with smooth surface and pinhole-free were obtained on ITO glass through effectively controlling the morphology in air under the relative humidity of lower than 30%. PCBM was used as the electron transport material, and devices with the structure of ITO/$CH_3NH_3PbI_3$/PCBM/Al were

[a] *CAS Key Laboratory of Bio-based Materials, Qingdao Institute of Bioenergy and Bioprocess Technology, Chinese Academy of Sciences, Qingdao 266101, China.yangrq@qibebt.ac.cn (R. Yang).*

[b] *College of Materials Science and Engineering, Qingdao University of Science and Technology, Qingdao 266042, China.*

[c] *Department of Physics, Ocean University of China, Qingdao 266100, China.*

Electronic Supplementary Information (ESI) available: Materials, device fabrication and characterization, additional SEM, AFM and PL lifetime and stabilised power output data. See DOI: 10.1039/x0xx00000x

fabricated. The device shows PCE of 12.78% under the illumination of AM 1.5G, 100 mW $cm^2$, which is the highest reported value to date for perovskite solar cells without any hole transport layer in inverted structures.

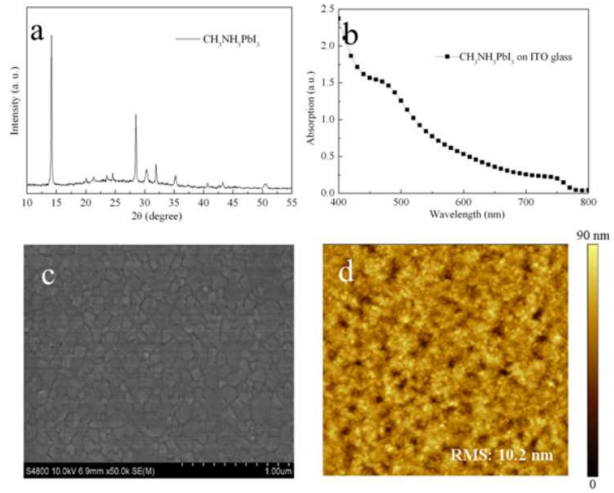


Figure 1. (a) XRD pattern, (b) Absorption spectrum (c) SEM image, and (d) AFM image (5 μm×5 μm) of perovskite film on ITO glass.

X-ray diffraction measurement was carried out to verify the structure and crystallization of the prepared film, as shown in Figure 1a. The XRD pattern of the prepared film has three intense diffraction peaks at 14.17°, 28.49° and 31.92°, which can be assigned to (110), (220) and (310) crystal planes of the tetragonal perovskite structure, respectively [8]. There are no impurity peaks in the XRD pattern of the $CH_3NH_3PbI_3$ film, indicating that the $PbI_2$ and $CH_3NH_3I$ have completely transformed into perovskite phase. Figure 1b shows the typical absorption spectrum of the $CH_3NH_3PbI_3$ perovskite film on ITO substrate, which absorbs a wide range from visible to near infrared as previous reported [26]. The surface quality of perovskite film is extremely important for high-performance solar cells applications. To evaluate the morphology of the prepared $CH_3NH_3PbI_3$ perovskite film on ITO glass, the scanning electron microscopy (SEM) was employed to investigate the surface morphology, as shown in Figure 1c. It clearly shows that the perovskite film is composed with compact grains with the size of a few hundred nanometers and full coverage on the ITO glass. Furthermore, it exhibits large homogeneous film without any cracks (Figure S1a, Supporting Information). It is worth pointing out that there are no pinholes, which could reduce photocurrent recombination between two electrodes. The film was further characterized by tapping-mode atomic force microscopy (AFM) as shown in Figure1d. The film shows flat surface morphology with the root mean square (RMS) roughness of 10.2 nm for area of 5 μm×5 μm. Even enlarging scanning area to 10 μm×10 μm (Figure S1b), the RMS value is still only 10.7 nm. The quite smooth surface is favorable to cover with a thin layer of electron transport layer, such as PCBM for inverted structures or Spiro-OMeTAD for conventional devices.

The sandwich-structure inverted perovskite solar cell with the configuration of glass/ITO/$CH_3NH_3PbI_3$/PCBM/Al (Figure 2a) without using hole transport layer was designed and fabricated, and its cross section scanning electron microscopy (SEM) image is shown in Figure 2a. From the cross section view, there are no clear crystalline grain boundaries, cracks or pinholes in the perovskite layer. It can be seen that the device shows a flat layer-by-layer structure with clear interfaces. The thickness of perovskite film is about 270-300 nm, which is adequate to absorb incident light sufficiently[39]. Furthermore, photo-induced carriers can be effectively collected due to their long lifetimes and excellent transport properties [13,14]. The smooth surface of perovskite film discussed above, can be fully covered by 40 nm thickness PCBM film. It is known to all that the energy-level matching is very important for high-performance devices. A schematic energy diagram of the device is illustrated in Figure 2b. The lowest unoccupied molecular orbital (LUMO) and the highest occupied molecular orbital (HOMO) levels of $CH_3NH_3PbI_3$ and PCBM were taken from the literature values [40,41]. When light irradiates on the solar cells, the $CH_3NH_3PbI_3$ layer will absorb photons to produce carriers, and the carriers will diffuse to corresponding electrodes to be collected. As shown in Figure 2b, because the LUMO level of $CH_3NH_3PbI_3$ is higher than that of PCBM, efficient electron transport to Al cathode is expected. Meanwhile, the work function of ITO and the HOMO level of $CH_3NH_3PbI_3$are -4.7 eV and -5.46 eV, respectively. From the viewpoint of energy levels, the device should exhibit high hole transport and collection efficiency to ITO electrode. In addition, steady-state photoluminescence (PL) spectra of perovskite film on glass and ITO with the photoexcitation at 507 nm are recorded and shown in Figure 2c. There is a sharp PL spectrum at 770 nm for the film prepared on glass substrate, which is consistent with the previous reported results [42]. However, a significant quenching effect was observed in the film on ITO substrate. The result further confirms that the holes can be effectively transferred at the interface of ITO and $CH_3NH_3PbI_3$. Furthermore, the PL lifetime of $CH_3NH_3PbI_3$ film on ITO substrate was also investigated (Figure S2). According to previous report, the PL lifetimes of neat $CH_3NH_3PbI_3$ film and $CH_3NH_3PbI_3$/PEDOT:PSS are 200.1 and 50 ns, respectively. Here, the PL lifetime of $CH_3NH_3PbI_3$ film is only 28.5 ns, indicating that the charge transfer fast even without PEDOT:PSS layer.

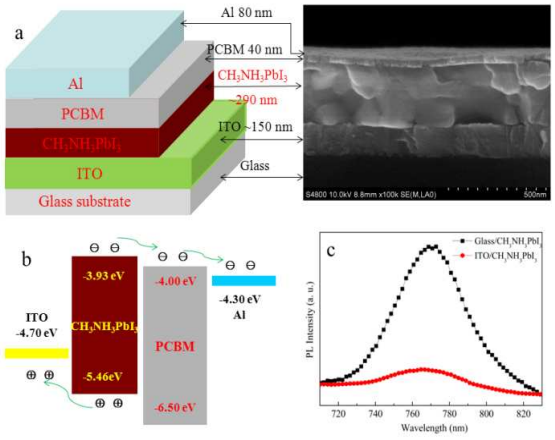


Figure 2 (a) Schematic device architecture and SEM cross sectional image of the device, (b) energy band diagram of perovskite solar

cell, (c) steady-state PL spectra of perovskite film on ITO and glass with photoexcitation at 507 nm.

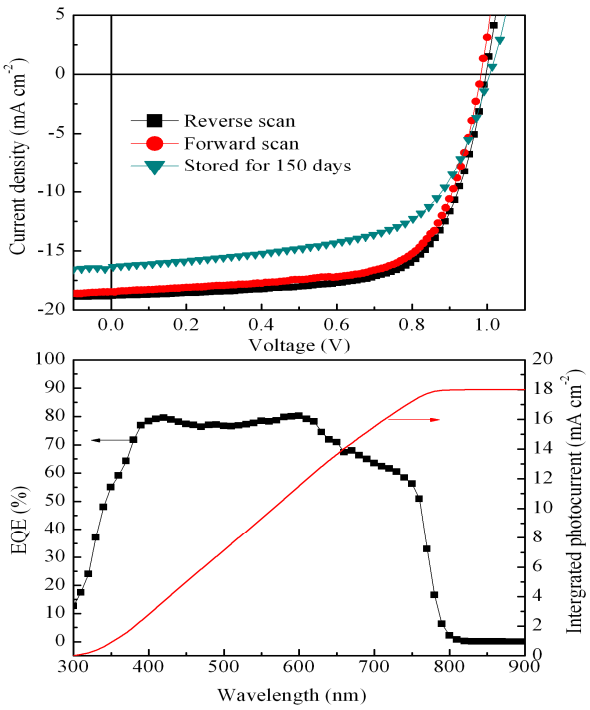


Figure 3. (a) *J–V* characteristics of the device measured by reverse and forward scans, and stored for 150 days (b) the EQE curve and integrated photocurrent for the device.

The typical current density–voltage (*J–V*) curves of the perovskite solar cells were measured under the irradiation of AM 1.5G, 100 mW cm$^{-2}$ and with the scan rate of 100 ms/10 mV, as shown in Figure 3a. The device performance parameters were summarized in Table 1. The device exhibits good PCE of 12.78%, with a high open circuit voltage ($V_{OC}$) of 0.997 V, a short circuit current density ($J_{SC}$) of 18.83 mW cm$^{-2}$ and a fill factor (FF) of 68.04%. In addition, forward *J–V* scan is also given in Figure 3a. The PCE of 12.21% is obtained and the hysteresis is negligible. The results demonstrate that the holes can be effectively transported and collected, and consequently the device exhibits high-performance even without any hole transport layer. Moreover, the stability was investigated with the devices stored for 150 days. The obtained *J–V* curve and related device parameters were also given in Figure 3a and Table 1. The device shows good stability with its PCE of 9.91% after stored for 150 days, only drops 23%. In our previous result, the PCE drops 12.3% after 20 days for the devices include a PEDOT:PSS hole transporter [43]. The improved device stability could be due to without application of PEDOT:PSS layer. Furthermore, the current and power output of the devices without or with PEDOT: PSS layer were given in Figure S3. The solar cells with different structures show similar in stabilized power output in comparison with the *J-V* curves with reverse scan. As we know that the stabilized power output was poor for hole/electron transport layer free devices in the previous reports [23, 44]. The excellent stabilized power output could be due to the improved the quality of $CH_3NH_3PbI_3$ layer and formed good contact with ITO glass.

Furthermore, in order to verify the accuracy of the *J–V* values, the corresponding external quantum efficiency (EQE) of the perovskite solar cell was measured, as shown in Figure 3b. The device exhibits excellent photo-response in the broad range of 350-750 nm with the maximum EQE of 80.17% at 600 nm. The cut-off of the photo-response is at 790 nm, which agrees well with the optical band gap of $CH_3NH_3PbI_3$ (Figure S2). Importantly, the calculated $J_{SC}$ from the integrating EQE spectrum is 17.98 mW cm$^{-2}$, which is coincident with the measured value of 18.83 mA/cm$^2$.

Table 1 Device performance parameters of the perovskite solar cells

| | $V_{OC}$ (V) | $J_{SC}$ (mA cm$^{-2}$) | FF (%) | PCE (%) |
|---|---|---|---|---|
| Reverse scan | 0.997 | 18.83 | 68.04 | 12.78 |
| Forward scan | 0.984 | 18.44 | 67.32 | 12.21 |
| Store [a] | 1.006 | 16.36 | 60.19 | 9.91 |
| Average [b] | 0.973 | 16.52 | 67.57 | 10.85 |

[a] The device stored for 150 days in glovebox; [b] the values taken from 60 separate devices.

In order to investigate the reproducibility of the cells, 60 separate devices were fabricated and tested using the previous optimization conditions. Figure 4 shows the histograms of the device performance parameters. Gaussian fit of the distribution was plotted for the histogram. As can be seen from Figure 4b, all devices show relatively high $V_{OC}$ of nearly 1.00 V. The $V_{OC}$ is higher than those of the previous reported devices with PEDOT:PSS as hole transport layer, which is mainly ascribed to high-quality perovskite film and matching the work function of ITO electrode [28]. In addition, the average $J_{SC}$ is moderate with the value of nearly 17.00 mW cm$^{-2}$, and the FF is very good (~70%) for all devices. As a result, the 60 separate devices show average PCE as high as 10.85% (Table 1). As we know that the high performance is related to energy level matches of devices, good morphology and long carrier lifetimes of perovskite film. As discussed above, the perovskite film directly prepared on ITO is smooth and pinhole-free and it can be fully covered with a thin layer PCBM, together with appropriate energy level matching, resulting in high photovoltaic performance without PEDOT:PSS layer.

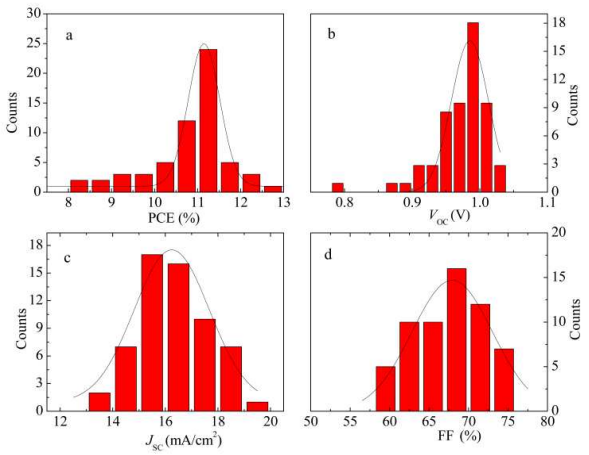

Figure 4. Histogram of PCE, $V_{OC}$, $J_{SC}$, and FF for 60 devices

## Conclusions

In conclusion, we fabricated an inverted planar perovskite solar cell directly on ITO glass without using any hole transport layer. Through effectively controlling the morphology, the perovskite films with flat surface and pinhole-free were prepared on ITO glass. From the viewpoint of device energy level and PL results, efficient charge extraction has occurred at the both of $CH_3NH_3PbI_3$/PCBM and ITO/$CH_3NH_3PbI_3$ interfaces. In combination with high charge carrier mobility of the excellent perovskite film, the PCE of 12.78% was obtained under the illumination of AM 1.5G, 100 mW/cm$^2$ in an inverted perovskite solar cell without hole transport layer. The results indicate that perovskite films directly preparing on ITO without any hole transport layer can also produce high-performance perovskite solar cells. It provides an attractive alternative for easy processing large scale fabrication of low-cost perovskite solar cells.

## Acknowledgments

This work was supported by the Ministry of Science and Technology of China (2014CB643501, 2010DFA52310), the National Natural Science Foundation of China (61107090, 51173199, 41172110 and 21274161), and Key Laboratory of Infrared Imaging Materials and Detectors, Shanghai Institute of Technical Physics, Chinese Academy of Sciences (IIMDKFJJ-14-08).

## Notes and references

1 Y. Liu, J. Zhao, Z. Li, C. Mu, W. Ma, H. Hu, K. Jiang, H. Lin, H. Ade and H. Yan, *Nat. commun.*, 2014, **5**, 5293.
2 Z. He, C. Zhong, X. Huang, W. Y. Wong, H. Wu, L. Chen, S. Su and Y. Cao, *Adv. Mater.,*2011, **23**, 4636–4643.
3 J. You, L. Dou, K. Yoshimura, T. Kato, K. Ohya, T. Moriarty, K. Emery, C. C. Chen, J. Gao, G. Li and Y. Yang, *Nat. commun.*, 2013, **4**, 1446.
4 X. Bao, Q. Zhu, T. Wang, J. Guo, C. Yang, D. Yu, N. Wang, W. Chen and R. Yang, *ACS Appl. Mater. Interfaces*, 2015, **7**, 7613–7618.
5 M. Wang, M. Xu, D. Shi, R. Li, F. Gao, G. Zhang, Z. Yi, R. Humphry-Baker, P. Wang, S. M. Zakeeruddin and M. Grätzel, *Adv. Mater.*, 2008, **20**, 4460–4463.
6 Z. Yao, M. Zhang, H. Wu, L. Yang, R. Li and P. Wang, *J. Am. Chem. Soc.*, 2015, **137**, 3799–3802.
7 M. Yuan, D. Zhitomirsky, V. Adinolfi, O. Voznyy, K. W. Kemp, Z. Ning, X. Lan, J. Xu, J. Y. Kim, H. Dong and E. H. Sargent, *Adv. Mater.*, 2013, **25**, 5586–5592.
8 J. Burschka, N. Pellet, S. J. Moon, R. Humphry-Baker, P. Gao, M. K. Nazeeruddin and M. Gratzel, *Nature*, 2013, **499**, 316–319.
9 N. J. Jeon, J. H. Noh, Y. C. Kim, W. S. Yang, S. Ryu, and S. I. Seok, *Nat. Mater.*, 2014, **13**, 897–903.
10 D. Liu, T. L. Kelly, *Nat. Photon.*,2014, **8**, 133-138.
11 J. W. Lee, D. J. Seol, A. N. Cho and N. G. Park, *Adv. Mater.*, 2014, **26**, 4991–4998.
12 T. C. Sum and N. Mathews, *Energy Environ. Sci.*, 2014, **7**,2518–2534.
13 G. Xing, N. Mathews, S. Sun, S. S. Lim, Y. M. Lam, M. Gratzel, S. Mhaisalkar and T. C. Sum, *Science*, 2013, **342**, 344–347.
14 S. D. Stranks, G. E. Eperon, G. Grancini, C. Menelaou, M. J. Alcocer, T. Leijtens, L. M. Herz, A. Petrozza and H. J. Snaith, *Science*, 2013, **342**, 341–344.
15 A. Kojima, K. Teshima, Y. Shirai, T. Miyasaka, *J. Am. Chem. Soc.* 2009, **131**, 6050–6051.
16 S. Shi, Y. Li, X. Li and H. Wang, *Mater. Horiz.,* 2015, **2**, 378–405.
17 H. Zhou, Q. Chen, G. Li, S. Luo, T. Song, H. S. Duan, Z. Hong, J. You, Y. Liu, Y. Yang, *Science*, 2014, **345**, 542–546.
18 Q. Hu, J. Wu, C. Jiang, T. Liu, X. Que, R. Zhu, Q. Gong, *ACS Nano* 2014, **8**, 10161–10167.
19 N. J. Jeon, J. H. Noh, W. S. Yang, Y. C. Kim, S. Ryu, J. Seo and S. I. Seok, *Nature,*2015, **517**, 476–480.
20 W. S. Yang, J. H. Noh, N. J. Jeon, Y. C. Kim, S. Ryu, J. Seo, S. I. Seok, *Science*, 2015, **348**, 1234–1237.
21 J. M. Ball, M. M. Lee, A. Hey and H. J. Snaith, *Energy Environ. Sci.*, 2013, **6**, 1739–1743.
22 N. J. Jeon, H. G. Lee, Y. C. Kim, J. Seo, J. H. Noh, J. Lee, S. I. Seok, *J. Am. Chem. Soc*. 2014, **136**, 7837–7840.
23 H. J. Snaith, A. Abate, J. M. Ball, G. E. Eperon, T. Leijtens, N. K. Noel, S. D. Stranks, J. T. W. Wang, K. Wojciechowski and W. Zhang, *J. Phys. Chem. Lett.*, 2014, **5**, 1511–1515.
24 H. S. Kim and N. G. Park, *J. Phys. Chem. Lett.*, 2014, **5**, 2927–2934.
25 W. H. Nguyen, C. D. Bailie, E. L. Unger and M. D. McGehee, *J. Am. Chem. Soc.*, 2014, **136**, 10996–11001.
26 J. Y. Jeng, Y. F. Chiang, M. H. Lee, S. R. Peng, T. F. Guo, P. Chen and T. C. Wen, *Adv. Mater.*, 2013, **25**, 3727–3732.
27 C. Chen, S. Bae, W. Chang, Z. Hong, G. Li, Q. Chen, H. Zhou and Y. Yang, *Mater. Horiz.,* 2015, **2**, 203–211.
28 J. You, Z. Hong, Y. Yang, Q. Chen, M. Cai, T. B. Song, C.C. Chen, S. Lu, Y. Liu, H. Zhou, Y. Yang, *ACS Nano*, 2014, **8**, 1674–1680.
29 Y. Chen, T. Chen and L. Dai, *Adv. Mater.*, 2015, **27**, 1053-1059.
30 K. Wang, C. Liu, P. Du, J. Zheng, X. Gong, *Energy Environ. Sci.*, **2015**, 8, 1245–1255.
31 F. X. Xie, D. Zhang,H. Su, X. Ren, K. S. Wong, M. Grätzel, W. C. H. Choy, *ACS Nano,* **2015**, 9, 639–646.
32 P. W. Liang, C. Y. Liao, C. C. Chueh, F. Zuo, S. T. Williams, X. K. Xin, J. Lin, A. K. Y. Jen, *Adv. Mater.* 2014, **26**, 3748–3754.
33 K. W. Wong, H. L. Yip, Y. Luo, K. Y. Wong, W. M. Lau, K. H. Low, H. F. Chow, Z. Q. Gao, W. L. Yeung, C. C. Chang, *Appl. Phys. Lett*. 2002, **80**, 2788–2790.
34 G. Niu, W. Li, F. Meng, L. Wang, H. Dong, Y. Qiu, *J. Mater. Chem. A* 2014, **2**, 705–710.
35 X. Bao, L. Sun, W. Shen, C. Yang, W. Chen and R. Yang, *J. Mater. Chem. A*, 2014, **2**, 1732–1737.
36 J. Y. Jeng, K. C. Chen, T. Y. Chiang, P. Y. Lin, T. D. Tsai, Y. C. Chang, T. F. Guo, P. Chen, T. C. Wen and Y. J. Hsu, *Adv. Mater.*, 2014, **26**, 4107–4113.
37 K. C. Wang, P. S. Shen, M. H. Li, S. Chen, M. W. Lin, P. Chen and T. F. Guo, *ACS Appl. Mater. Interfaces*, 2014, **6**, 11851–11858.
38 W. Chen, Y. Wu, J. Liu, C. Qin, X. Yang, A. Islam, Y.-B. Cheng and L. Han, *Energy Environ. Sci.*, 2015,**8**, 629–640
39 C. R. Carmona, O. Malinkiewicz, R. Betancur, G. Longo, C. Momblona, F. Jaramillo, L. Camacho, H. J. Bolink, *Energy Environ. Sci.*, 2014,**7**, 2968–2973.
40 S. Ryu, J. H. Noh, N. J. Jeon, Y. C. Kim, W. S. Yang, J Seo, S. I. Seok, *Energy Environ. Sci.*, 2014, **7**, 2614–2618
41 B. Yin, L. Yang, Y. Liu, Y. Chen, Q. Qi, F. Zhang, S. Yin, Appl. Phys. Lett., 2010, **97**, 023303.
42 W. Zhang, M. Saliba, D. T. Moore, S. K. Pathak, M. T. Horantner, T. Stergiopoulos, S. D. Stranks, G. E. Eperon, J. A. Alexander-Webber, A. Abate, A. Sadhanala, S. Yao, Y. Chen, R. H. Friend, L. A. Estroff, U. Wiesner and H. J. Snaith, *Nat. commun.*, 2015, **6**, 6142.
43 X. Bao, Y. Wang, Q. Zhu, N. Wang, D. Zhu, J. Wang, A. Yang, R. Yang, *J. Power Sources* 2015 **297** 53–58.



 

44 Y. Zhang, M. Liu, G. E. Eperon, T. C. Leijtens, D. McMeekin, M. Saliba, W. Zhang, M. Bastiani, A. Petrozza, L. M. Herz, M. B. Johnston, H. Lin, H. J. Snaith, *Mater. Horiz.* 2015, 2,315–322.

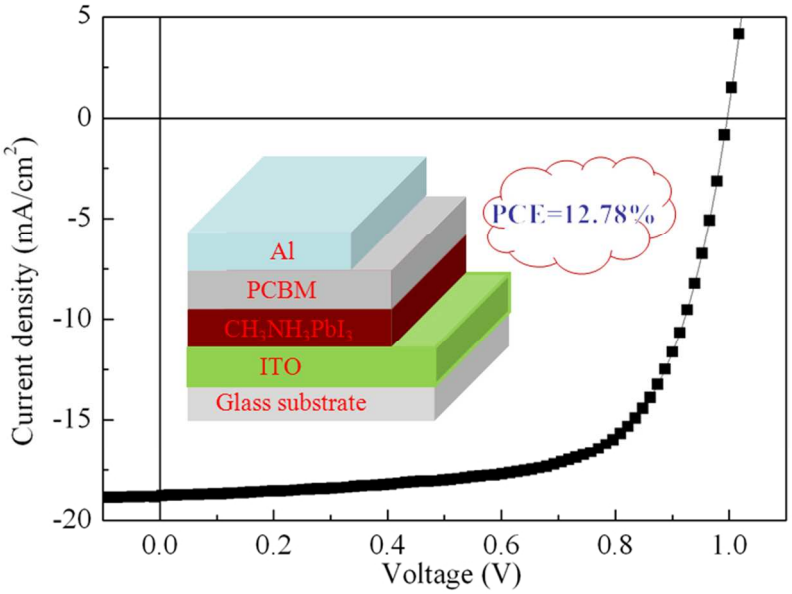


254x190mm (96 x 96 DPI)